

# Performance Measurements and Technology Demonstration of the VASIMR<sup>®</sup> VX-200

Edgar A. Bering, III<sup>1</sup>

*University of Houston, Department of Physics, Houston, TX 77204, USA*

Benjamin W. Longmier<sup>2</sup>, Jared P. Squire<sup>2</sup>, Tim W. Glover<sup>3</sup>, Leonard D. Cassady<sup>4</sup>, Andrew V. Ilin<sup>5</sup>, Mark D. Carter<sup>6</sup>,  
Chris S. Olsen<sup>7</sup>, Greg E. McCaskill<sup>8</sup>, and Franklin R. Chang Diaz<sup>9</sup>  
*Ad Astra Rocket Company, Webster, TX 77598, USA*

**Recent progress is discussed in the development of an advanced RF electric propulsion engine: the Variable Specific Impulse Magnetoplasma Rocket (VASIMR<sup>®</sup>) VX-200, a 200 kW flight-technology prototype. Results are presented from first stage only and first stage with booster stage experiments that were performed on the VX-200 using between 60 mg/s and 150 mg/s argon propellant. Measurements of ion flux, ion energy, plasma density and potential gradients, and force density profiles taken in the exhaust plume of the VX-200 are made within a 150 cubic meter vacuum chamber and are presented in the context of individual stage and total engine performance. An emphasis will be given to the current status of technology innovation that makes the ground based VX-200 and the ISS mounted VF-200 engines possible.**

## Nomenclature

$\eta_A$	=	ICH coupler efficiency
$\eta_b, \eta_B$	=	ion coupling efficiency. Percent of second stage coupled RF power that becomes directed kinetic energy
$\eta_n$	=	nozzle efficiency
$\eta_T$	=	thruster efficiency
$e$	=	electron charge
$E_1$	=	kinetic energy of ions exiting first stage
$E_2$	=	kinetic energy of ions owing to 2 <sup>nd</sup> stage boost
$E_i$	=	ionization cost of the helicon stage
$f$	=	frequency
$f_{ci}$	=	ion cyclotron frequency
$F$	=	ion velocity phase space distribution function
$F_T$	=	total force measured in the plume
$\Gamma, \Gamma_i$	=	total ion flux through the rocket
$g$	=	acceleration of gravity
$I_{sp}$	=	specific impulse
$L_A$	=	inductance of the ICH coupler

<sup>1</sup> Professor, Physics and ECE, 617 Science & Research I /PHYS 5005, Associate Fellow

<sup>2</sup> Research Scientist, Ad Astra Rocket Company, 141 W. Bay Area Blvd. Member

<sup>2</sup> Director of Research, Ad Astra Rocket Company, 141 W. Bay Area Blvd. Member

<sup>3</sup> Director of Development, Ad Astra Rocket Company, 141 W. Bay Area Blvd., Member

<sup>4</sup> Lead Project Engineer, Ad Astra Rocket Company, 141 W. Bay Area Blvd. Member

<sup>5</sup> Computational Research Lead, Ad Astra Rocket Company, 141 W. Bay Area Blvd.

<sup>6</sup> Director of Technology, Ad Astra Rocket Company, 141 W. Bay Area Blvd.

<sup>7</sup> Research Scientist, Ad Astra Rocket Company, 141 W. Bay Area Blvd.

<sup>8</sup> Senior RF Engineer, Ad Astra Rocket Company, 141 W. Bay Area Blvd., Member

<sup>9</sup> Chief Executive Officer, Ad Astra Rocket Company, 141 W. Bay Area Blvd., Associate Fellow

$L_M$	=	inductance of the ICH coupler matching network
$\dot{m}$ , $m_{dot}$	=	propellant (argon) mass flow rate
$m_{Ar}$	=	mass of an argon atm
$P_{1,RF}$	=	RF power coupled into ions in the first stage
$P_{plasma}$	=	ICH RF power broadcast into plasma
$P_{2,RF}$ , $P_{ion}$	=	ICH RF power coupled into ions in the second stage
$P_{ICH}$	=	ICH RF power into coupler
$P_{jet}$	=	thruster jet power
$Q_c$	=	quality factor of the ICH coupler circuit
$R_c$	=	resistance of the ICH coupler circuit
$R_p$	=	plasma loading of the ICH coupler
$\Theta$	=	pitch angle
$\theta$	=	half angle of the plume divergence
$v_{ICRF}$	=	exhaust plasma flow velocity with ICH on
$v_{helicon}$	=	exhaust plasma flow velocity with helicon only
$VSWR_{plasma}$	=	voltage standing wave ratio of the ICH coupler, with plasma present
$VSWR_{vacuum}$	=	voltage standing wave ratio of the ICH coupler, with no plasma present
$W_{ICH}$	=	mean ion energy increase owing to ICH
$\omega$	=	angular frequency

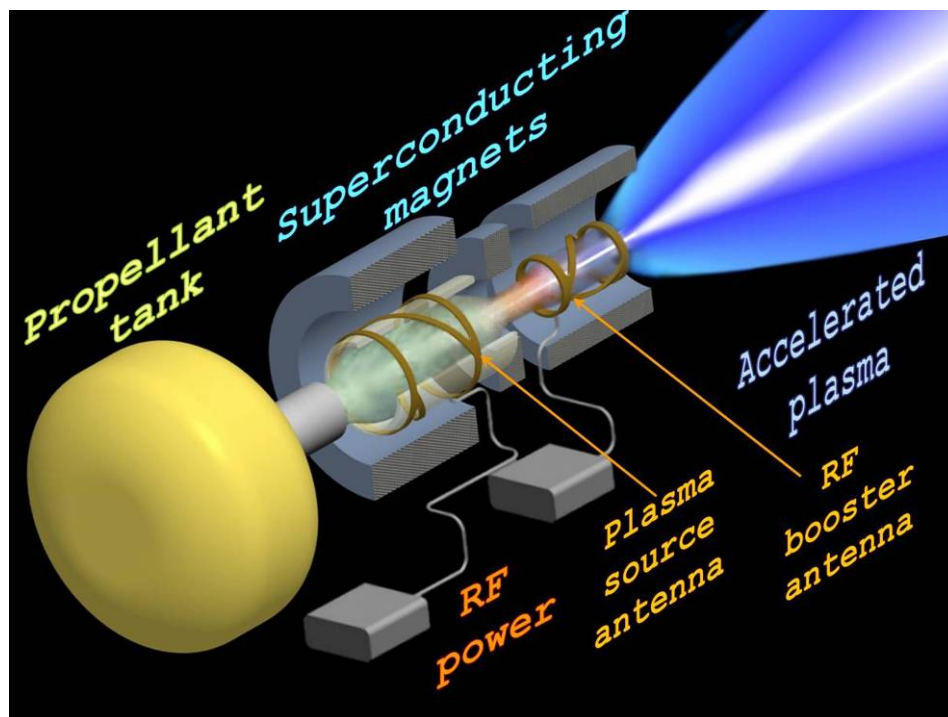


Figure 1. A cartoon of the VASIMR<sup>®</sup> system, illustrating the basic concepts.

## I. Introduction

THE exploration of the solar system will be one of the defining scientific tasks of the new century. One of the obvious challenges faced by this enterprise is the scale size of the system under study,  $10^{11}$  -  $10^{14}$  m. Over distances on this scale and given the performance of present day rockets, the mission designer is faced with the choice of accepting multi-year or even decadal mission time lines, paying for enormous investment in rocket propellant compared to useful payload, or finding a way to improve the performance of today's chemical rockets. For human space flight beyond Earth's orbit, medical, psychological, and logistic considerations all dictate that drastic thruster improvement is the only choice that can be made. Even for robotic missions beyond Mars, mission

time lines of years can be prohibitive obstacles to success, meaning that improvements in deep space sustainer engines are of importance to all phases of solar system exploration<sup>1</sup>.

High-power electric propulsion systems have the capability of reducing the propellant mass for heavy-payload orbit raising missions and cargo missions to the moon and can even reduce the trip time of piloted planetary missions<sup>1,2,3,4,5,6</sup>. The VArIable Specific Impulse Magnetoplasma Rocket (VASIMR<sup>®</sup>), is one of the few electric propulsion devices capable of processing a great power densities ( $\sim 6 \text{ MW/m}^2$ ) with an expected long lifetime. A simplified concept is shown in Figure 1. The advantages of the VASIMR<sup>®</sup> are high power, high specific impulse, constant power variable specific impulse, and potentially long lifetime due to the magnetic containment of the plasma stream. The rocket relies on efficient plasma production in the first stage using a helicon plasma source<sup>7,8</sup>. Ion cyclotron resonance enables efficient ion heating in the second stage (RF booster). Thrust is realized in the final stage as the plasma accelerates in a magnetic nozzle. End-to-end testing of the VASIMR<sup>®</sup> with a space flight-like configuration, the optimum magnetic field configuration, and a vacuum facility large enough and with enough pumping to allow for plume measurements with low background pressure was only achieved recently.

The VASIMR<sup>®</sup> engine has three major subsystems, the plasma generator stage, the RF “booster” stage and the nozzle, shown in Figure 1. The details of the engine and its design principles have been previously reported<sup>9,10</sup>. The first stage is a helicon discharge that has been optimized for maximum power efficiency (lowest ionization cost in eV/(electron-ion pair)<sup>7,8,11,12,13</sup>. The next stage downstream is the heating system. Energy is fed to the system in the form of a circularly polarized RF signal tuned to the ion cyclotron frequency. ICH heating has been chosen because it transfers energy directly and largely to the ions, which maximizes the efficiency of the engine<sup>14,15</sup>. In the present small-scale test version, there is no mirror chamber and the ions make one pass through the ICH coupler. The system also features a two-stage magnetic nozzle, which accelerates the plasma particles by converting their azimuthal energy into directed momentum. The detachment of the plume from the field takes place mainly by the loss of adiabaticity and the rapid increase of the local plasma  $\beta$ , defined as the ratio of the plasma to the magnetic pressures.

Ad Astra Rocket Company has been hard at work improving the VASIMR<sup>®</sup> design and plume diagnostics in order to measure rocket performance at 200 kW. Previous versions of the VASIMR<sup>®</sup> and limitations of the vacuum facility hindered the effort to accurately measure performance<sup>16,17,18</sup>. The most recent technical publications do not show full power operation at 200 kW, nor was there enough plume data to calculate thrust efficiency<sup>19,20,21,22</sup>.

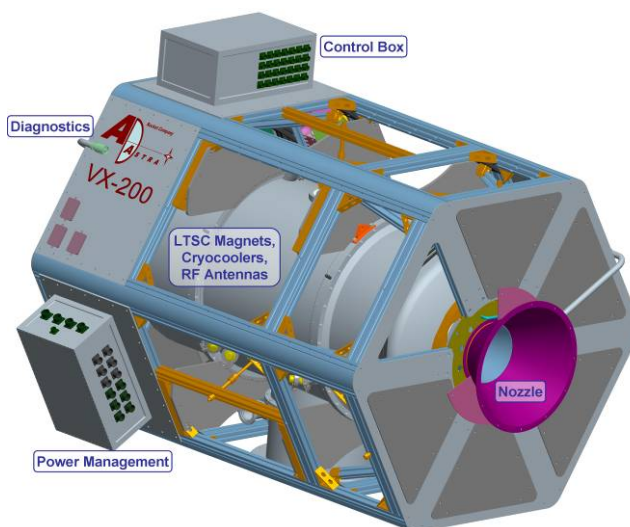
The VX-200 is a 200kW VASIMR<sup>®</sup> engine prototype currently in the early stages of the testing phase. The VX-200, completed in May of 2009, is considered by company officials to be the last step before construction of the VF-200 (for VASIMR<sup>®</sup> flight) series of flight engines planned for space testing in 2014. In this paper we use VX-200 test data to demonstrate that a VASIMR<sup>®</sup> in a configuration similar to a space flight design can operate at 200 kW and efficiently (greater than 50%) produce force in the specific impulse range of interest. This paper primarily presents experimental results recorded over the past year that benefit from a high-quality vacuum facility with excellent plume diagnostics. Plasma flux, RF power measurements, and neutral argon gas flow rate measurements, combined with knowledge of the kinetic energy of the ions leaving the rocket are used to show ionization cost of the argon, force produced by the thruster, and the thrust efficiency. Here we present experimental data that demonstrate performance above 100 kW with the best operating conditions for which measurements have been obtained.

## II. Experimental Setup

### A. The VASIMR<sup>®</sup> Engine

#### 1. VX-200

The VX-200 is an experimental version of the VASIMR<sup>®</sup> engine that is designed to utilize 200 kW of input DC electrical power. The experimental rocket is an end-to-end test of the primary components in a vacuum environment with the goal of measuring and improving performance. Most components of the rocket are located within the vacuum chamber, with only the RF generators, magnet power supplies, and magnet cryocoolers at atmospheric pressure outside of the vacuum chamber. The superconducting magnets, structural components, rocket core, and many electronic components are operated within the chamber. Figure 2 shows an image of the VX-200 3-D CAD model and a picture of the rocket installed inside the vacuum chamber. A key subsystem of the VX-200 is the superconducting magnet with a maximum field of approximately 2 Tesla that allows for efficient containment and acceleration of the plasma. Another key subsystem is the rocket core - the components that physically surround the plasma and intercept the bulk of the waste heat.



(a) An image of the simplified 3-D model of the VX-200 with a point of view from the aft end.



(b) A picture of VX-200 installed in the large chamber at Ad Astra Rocket Company.

**Figure 2. Images of the VX-200**

The VX-200 is restricted to pulses of less than one minute in length owing to temperature limitations of certain seals and joints in the rocket core. We will use the pulsed operation thermal data to design the optimal thermal solution for the measured heat flux in future models. Most VX-200 pulses are between 1 and 15 seconds in length.

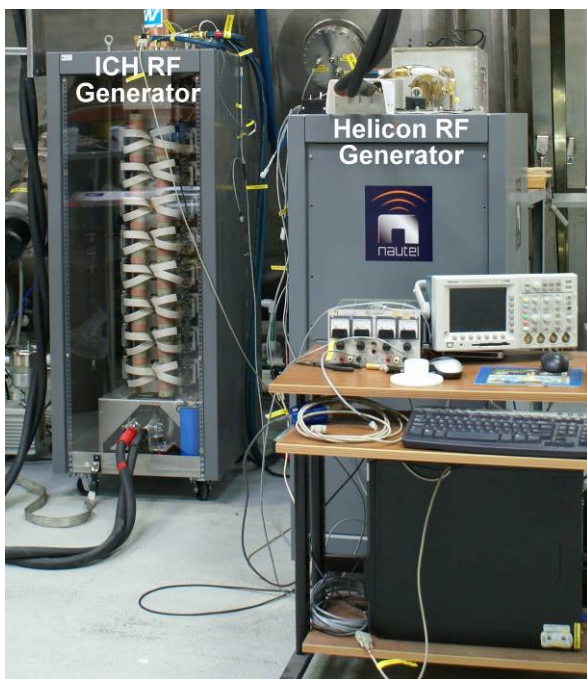


**Figure 3. A picture of ICH RF generator and the helicon RF generator.**

The VX-200 has a total RF power capability of 200 kW driven by high-efficiency, as high as 98%, solid-state DC-RF generators, as shown in Figure 3. The first stage, or helicon stage, launches a right-hand circularly polarized wave into the plasma. The plasma diameter is reduced by more than a factor of 2 as it flows downstream through a magnetic choke and containment wall that follows the plasma flux tube. Up to 40 kW of RF power (RF generator limited) can be deposited into 50 to 150 mg/s of flowing argon plasma. The helicon source internal structure was electrically floating. The second stage, or Ion Cyclotron Heating (ICH) stage, couples energy directly into the ions via ion cyclotron resonance with a wave that is launched into the plasma via a specially designed, proprietary coupler. The exhaust velocity of the ions increases as the RF power that is coupled into the ICH section increases. The primary components are the propellant flow controller, RF generators, rocket core, and magnet.

Argon gas flow control is provided by a Moog flow controller that can supply up to 150 mg/s. The other two components are described in the following subsections.

## 2. RF Generators

The VX-200 utilizes two solid-state RF generators developed by Nautel Limited of Canada specifically for this application. The helicon section RF generator converts power supplied at 375 VDC into approximately the industrial standard of 6.78 MHz RF with an efficiency of greater than 92% at up to 40 kW. The specific mass of the helicon section RF generator is less than 1 kg/kW. The ICH section RF generator converts power supplied at 375 VDC into ~500 kHz RF with an efficiency of greater than 98% at up to 170 kW. The specific mass of the ICH section RF generator is less than 0.5 kg/kW. These RF generators are not located within the vacuum chamber, but transmit the RF power into the vacuum chamber to the VX-200 through high-voltage, high-power RF feedthroughs. The components of the generators were not designed to operate in vacuum to enable timely testing of the VX-200.

## 3. Low Temperature Superconducting Magnet

The VASIMR<sup>®</sup> relies on magnetic fields to limit plasma erosion of the surrounding materials as well as to provide the field strength necessary for ion cyclotron resonance at a frequency that does not excessively excite electrons and limits the cyclotron radius. The gyroradius should be much less than the plasma radius, which corresponds to field strength of greater than 1 T. In order to have an efficient electric propulsion device, the magnet must consume a small amount of power compared to thrust power. The only feasible method to generate such a strong magnetic field is with a superconducting magnet. The VX-200 utilizes a state-of-the-art low temperature superconducting magnet designed and developed by Scientific Magnetics, LLC of the United Kingdom specifically for the VX-200. The magnet is shown in Figure 4. The space flight VASIMR<sup>®</sup> will utilize a high temperature superconducting magnet so that the heat-rejection systems that chill the magnet can operate at higher efficiency.



**Figure 4. The low temperature superconducting magnet with alignment fixtures mounted to the ends.**

## 4. Rocket Core

The rocket core is the most critical subsystem of the VASIMR<sup>®</sup> as it must protect the first and second stage RF couplers from the plasma, allow the RF to transmit with low loss to the plasma from the couplers, conduct many kilowatts of heat away from the plasma facing walls and magnets, and survive for tens of thousands of hours. Presently, Ad Astra is testing various configurations of the core to measure heat flux from the plasma and to find the best materials and layouts for steady-state operation at full power.

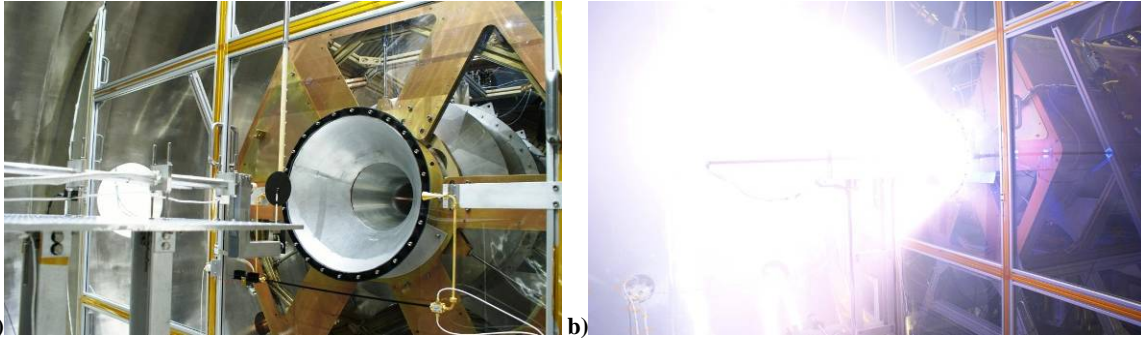


Figure 5. Photograph of the VX-200 rocket exhaust end facing the diagnostics platform (a), and a high power firing of the VX-200 with immersed plasma diagnostics at closest approach (b).



Figure 6 A picture of the “El Monstro” large vacuum chamber at Ad Astra Rocket Company.

## B. Vacuum Facility

Ad Astra Rocket Company operates a stainless steel vacuum chamber (see Figure 5, 6) designed for testing the VASIMR<sup>®</sup> engine. The vacuum chamber is 4.2 m in diameter and 10 m long with a volume of 150 m<sup>3</sup> (including the end caps). One end opens fully for access to the entire inner diameter. The vacuum chamber is partitioned into two sections, a rocket section and an exhaust section as shown in Figures 5-7. The rocket section stays at a lower pressure than the exhaust section while the VX-200 is firing. The partitioning was done to prevent arcing and glow discharges near the high voltage transmission lines and matching circuit components. There is a 2.5 m by 5 m translation stage that carries a suite of plasma diagnostics for plume characterization. The translation stage uses 2 independent ball screws and is driven by vacuum compatible stepper motors which yield a positional resolution of 0.5 mm. The facility has the capability of pumping 200,000 liters/s argon and 300,000 liters/s nitrogen with four PHPK Technologies CVI Torr Master<sup>®</sup> internal cryopumps. The exhaust section pressure is low enough (less than  $1 \times 10^{-5}$  torr) for the first 0.8 s of operation that collisions with background neutral gas do not affect the results. The

pressure is less than  $1 \times 10^{-7}$  torr before each shot. The pressure rises to a maximum of  $2 \times 10^{-4}$  torr after the rocket has been operating for more than 0.8 s.

a)

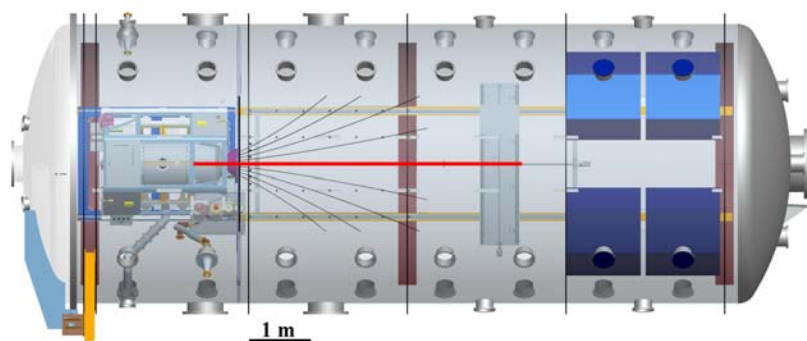


Figure 7. A CAD rendering of the VX-200 rocket bus mounted within the 150 m<sup>3</sup> Ad Astra Rocket Company high vacuum facility with superimposed vacuum magnetic field lines (a), and a photograph of the VX-200 rocket (background) and diagnostics platform (foreground) mounted on a 2 m by 5 m translation stage (b).

### C. Diagnostics

Plasma diagnostics include a triple probe, 32 and 70 GHz density interferometers, a bolometer, a television monitor, an H- $\alpha$  photometer, a spectrometer, neutral gas pressure and flow measurements, several gridded energy analyzers (retarding potential analyzer or RPA)<sup>3,8,23,24,25,26,27,28,29</sup>, a momentum flux probe<sup>30</sup>, an emission probe, a directional, steerable RPA and other diagnostics<sup>31</sup>. Two 10-probe arrays of fixed bias flux probes and a density interferometer are the primary plasma diagnostics. The flux probe arrays measure ion current profiles, calibrated by the density interferometer. An array of thermocouples provides a temperature map of the system.

Measurements of the plasma potential, electron temperature and ion density in the VX-200 rocket core and the plasma plume were made with a 1/4" diameter tungsten Langmuir probe with a guard ring, Figure 8. The probe was swept in voltage from -40 V to +40 V through the entire range of ion saturation and electron saturation regions with a sweep rate of 80 Hz and a sampling rate of 40 kHz. RF compensation was tested, and produced only 0.2 V variations in the measured plasma potential, and 0.1 eV variations in the electron temperature. Floating potential measurements were made with a high impedance oscilloscope from 1 Hz to 100 MHz. Fluctuations in the floating potential were observed to have maximum peak-to-peak amplitude of 0.4 V at the driving frequency of the helicon plasma source, near the industrial standard 6.78 MHz.

Measurements of the ion flux presented in this paper were taken with an array of ten 0.25 inch diameter molybdenum planar probes of a top hat design that were biased into the ion saturation regime, -15 V with respect to chamber ground, during VX-200 operation<sup>32</sup>. Occasionally, full I-V traces were taken and analyzed so that we could be sure that the probes were properly biased. Ion flux measurements were taken both during quick startup shots, where the ambient neutral gas pressure was below  $1 \times 10^{-5}$  Torr, and during translating radial profiles where the sustained neutral argon pressure within the vacuum chamber was below  $2 \times 10^{-4}$  Torr.

#### 1. Retarding potential analyzer (RPA)

Retarding potential analyzer (RPA) diagnostics have been installed to measure the accelerated ions. Measurements of the ion energy in the downstream section of the VX-200 plume were made with a cylindrical 4 2-layer grid RPA mounted on a powered goniometric hinge on the translation stage, to enable pitch angle scans. A four-grid configuration is used, with entrance attenuator, electron suppressor, ion analyzer and secondary suppressor grids. The grids were 49.2-wire/cm molybdenum mesh, spaced 1 mm apart with Macor spacers. The opening aperture is 1 cm in diameter, usually pointed at the plasma beam, mounted 0.1778 m from the center of the translation stage. For the results reported here, the VX-200 RPA did not have a front face collimator plate mounted.

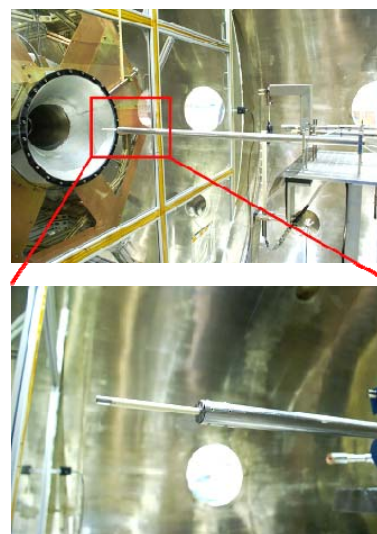


Figure 8. Photograph of a Langmuir probe with guard ring on a 70 cm extension shaft.

The interpretation of RPA output data in terms of ion energy requires an accurate knowledge of plasma potential ( $V_p$ ). When available, data from an RF compensated swept Langmuir probe provided by Los Alamos National Laboratory (LANL) are used to determine  $V_p$ . When other  $V_p$  data are not available, plasma potential is assumed to be the value at which  $dI/dV$  first significantly exceeds 0, which usually agreed with the LANL probe value within the error bars ( $\pm 5$  V). This value was typically  $\sim +0$ -50 V with respect to chamber ground in the VX-50. The operator biases the body and entrance aperture of the RPA to the observed plasma potential value. The ion exhaust parameters are deduced from the raw data by means of least squares fits of drifting Maxwellians to the current-voltage data<sup>29,31,33</sup>.

In this paper, the RPA data will be presented in several formats, including the voltage derivative of the I-V characteristic, the one-D ion velocity distribution function, a planar cut through the full ion velocity distribution function, and as derived parameters. The  $dI/dV$  plots (e.g. Figure 24) show the smoothed, numerically calculated derivative with respect to sweep voltage of the measured RPA current. Sweep voltage zero is set to plasma potential found using the methods of the previous paragraph, for ICH-off conditions and all other parameters unchanged. Unless stated otherwise, seventy-eight sweeps per shot of the RPA have been averaged to produce each VX-200 figure. The presence of features in the  $dI/dV$  curves at retarding voltages less than the plasma potential are the result of temporal fluctuations in the ion saturation current, and largely serve to illustrate the risks in taking numerical derivatives of data. The ion velocity distribution functions (e.g. Figure 25) were found from the  $dI/dV$  curves by dividing by the energy and multiplying by a calibration factor.

The RPA I-V characteristic data has been reduced by least-squares fitting the characteristic that would be produced by a drifting Maxwellian to the data. This fit has three parameters. The three free parameters in these fits are ion density, mean drift speed and the parallel ion temperature in the frame of reference moving with the beam. The temperature is found from these least squares fits, not from taking the slope of the logarithm of the data. The density is calibrated by comparison with nearby Langmuir probes and is probably best understood as a relative measurement. The temperature and ion drift speed parameters depend most strongly on the accuracy with which the retarding potential is known. The absolute uncertainty of the sweep voltage digitization with respect to chamber ground was a few percent when digitizer calibration uncertainty, sweep isolator reduction ratio precision and related parameters are folded in. There are systematic uncertainties associated with the determinations of plasma potential, which are discussed two paragraphs above. Plasma potential is always subtracted prior to any other analysis.

The full ion velocity phase space distribution function of the ions can be obtained by scanning the RPA in pitch angle between otherwise identical shots, assuming cylindrical (gyrotropic) symmetry<sup>34,35</sup>. The angle step size was  $5^\circ$  from  $0^\circ$  to  $50^\circ$  and  $10^\circ$  thereafter for all contour plot figures (Figure 25).

#### D. Force Target Construction and Operation

The force target, described in detail in an earlier publication<sup>30</sup>, consists of a 9-centimeter-diameter graphite target disc attached to a 10-centimeter-long insulating alumina rod. The stiff alumina rod then connects to a small titanium bar (5.72 cm x 1.30 cm) where a series of 4 high output semiconductor strain gauges, Micron Instruments model number SS-090-060-1150P, are mounted between two holes on an “isthmus” on the titanium bar, as seen in Figure 8, similar in design to earlier concepts<sup>36</sup>. The isthmus acts as a stress concentrator and increases the sensitivity of the device. The strain gauges are connected electrically in a Wheatstone bridge configuration so that changes in temperature of the titanium bar do not affect the linearity of the strain gauge output.

When the electrically floating graphite disc is immersed in flowing plasma (e.g. the plume of the VX-200) the force from the plasma impacting the graphite target is translated into a strain in the titanium beam through a moment arm equal to the length of the alumina rod plus the clamp length. A small graphite shield was also used to keep the

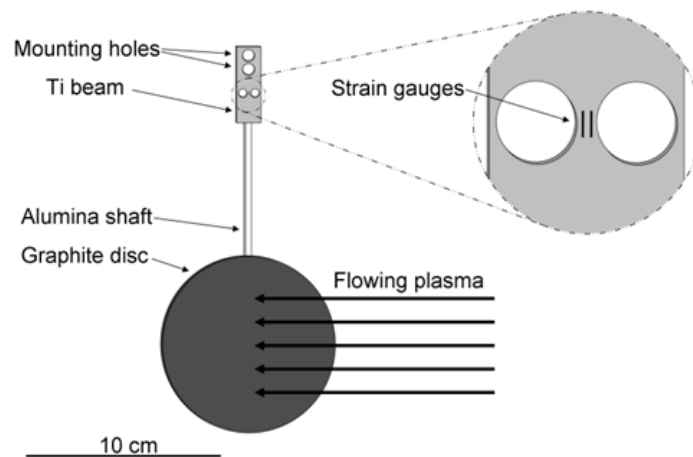


**Figure 9. A schematic of the force target assembly and magnification of strain gauge arrangement mounted on the titanium isthmus.**

entire titanium bar and strain gauge assembly shielded from the flowing plasma, and associated thermal and electrical noise. The resolution of the force target is 0.1 mN, which allowed for sufficiently sensitive measurements of the force applied by the exhaust plasma. The natural frequency of oscillations was 40 Hz, and this oscillation is filtered out during the analysis of radial or temporal force profiles, though the temporal data is limited in resolution to 1/40 s.

### III. Measurement of Ionization Cost

A key factor in maximizing the overall rocket efficiency is to create the plasma in the first stage with as little power as possible. The commonly used term for plasma generation efficiency is ionization cost and is presented as energy per ion in terms of electron volts. The VASIMR<sup>®</sup> helicon section has argon input into the upstream end and it flows to the ICH section. The RF power strips one electron of each ion. Power is lost through radiation from the excited argon neutrals and ions, flux of plasma to the walls where it recombines, and the frozen flow loss of ionization energy carried out of the helicon section. The ions also carry kinetic energy,  $E_i$ , but we do not count that as a loss since that energy represents thrust. Therefore the ionization cost is

$$E_i = \frac{P_{i,RF}}{\dot{m}} - E_1 \quad (1)$$

$m_{Ar}$

New measurements of the ionization cost were taken during helicon-only operation as a function of both RF power and argon propellant flow rate within the ranges of 15 to 35 kW and 50 to 150 mg/s, respectively. Ionization cost was determined by measuring the total ion flux from the VX-200 and then dividing the coupled RF power to the plasma by the total flux. Figure 10 is a contour map of the helicon performance as an ion source, and shows a clear

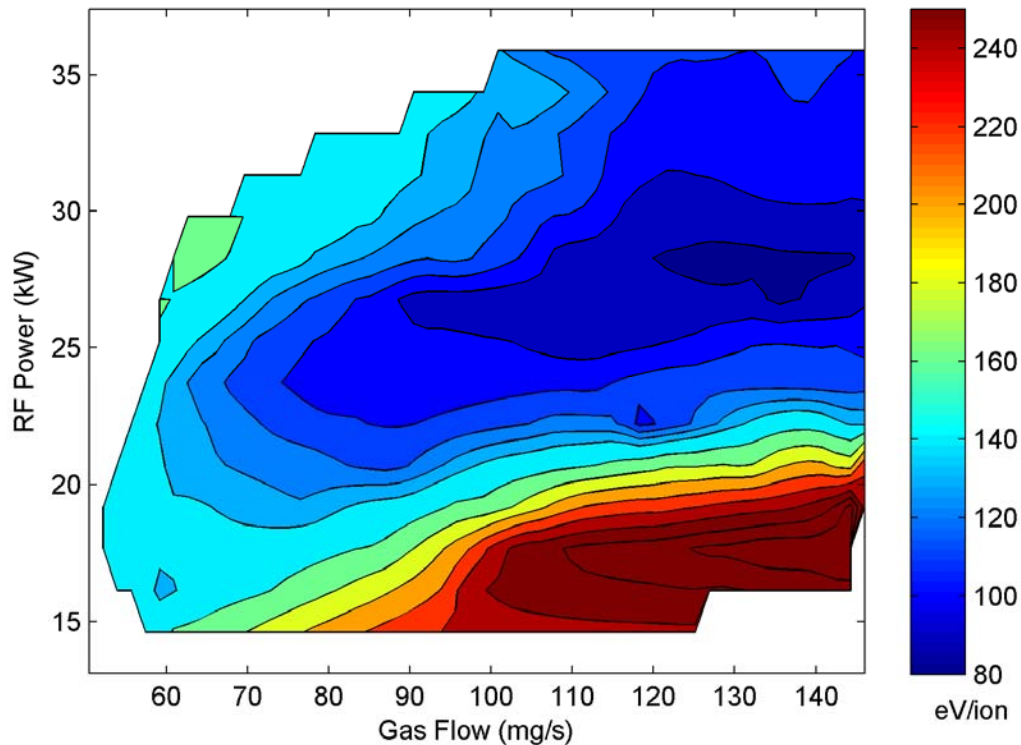


**Figure 10. A color contour plot of the ionization cost of the helicon stage as a function of both RF power and argon gas flow rate. The uncertainty of the ionization cost is 10%.**

indication of a valley of optimum ionization cost, as low as  $87 \pm 9$  eV per ion. Of course, each new core and helicon coupler will produce a unique ion cost performance map; though in general it is clear that providing too much propellant with too little RF power will result in an inefficient helicon plasma source. A scenario where there is too

little propellant and too much RF power will also result in inefficient helicon plasma source, though this region was out of range for the current setup because the plasma load changed too much for the matching circuit to compensate. Future experiment campaigns will look at constant power throttling of the VX-200, and this performance map provides a starting point for the operational settings of the helicon stage. A key point to remember with this ionization cost measurement is that this number is the cost of an ion that is actually extracted all the way through the rocket core, which is in many cases quite different from the ion cost directly within a helicon source tube as reported by many other university labs. The lowest ionization cost measurement of  $87 \pm 9$  eV occurred with VX-200 settings of 28 kW and 130 mg/s. Figure 11 shows the lowest ion cost measurements for each particular RF power setting, for which the flow rate is not fixed.

Exiting parallel ion energy for helicon-only operation was determined by using the measured total force and the measured total ionization fraction. The ionization fraction was determined by the ratio of the total measured ion current to that of the measured input propellant flow rate by a mass flow controller. During normal operation of the helicon source at 28 kW and 107 mg/s of argon flow, the measured ionization fraction within the exhaust plume, 40 cm downstream from the VX-200, was  $95\% \pm 5\%$ . Together with a total force measurement and a total coupled RF power measurement, a 95% ionization fraction yields an average parallel (axial) ion energy of  $12 \pm 1$  eV. This energy that the ions gain is likely due to an ambipolar ion acceleration process<sup>37</sup> as a result the expanding geometry of the magnetic field and a conversion of electron temperature into directed ion kinetic energy through a large scale axial electric field. No double layer structures were observed. We speculate that double layer structures require a much higher neutral gas pressure and, hence, the presence of downstream plasma source within the vacuum chamber. The neutral gas pressure during the flux measurements was held below  $1 \times 10^{-5}$  torr. It should also be noted that all plasma facing components within the VX-200 are electrically floating, an important distinction when discussing ion energy values with a thruster in a grounded chamber. Radial flux maps, Figure 12a, and radial force maps, Figure 12b, give

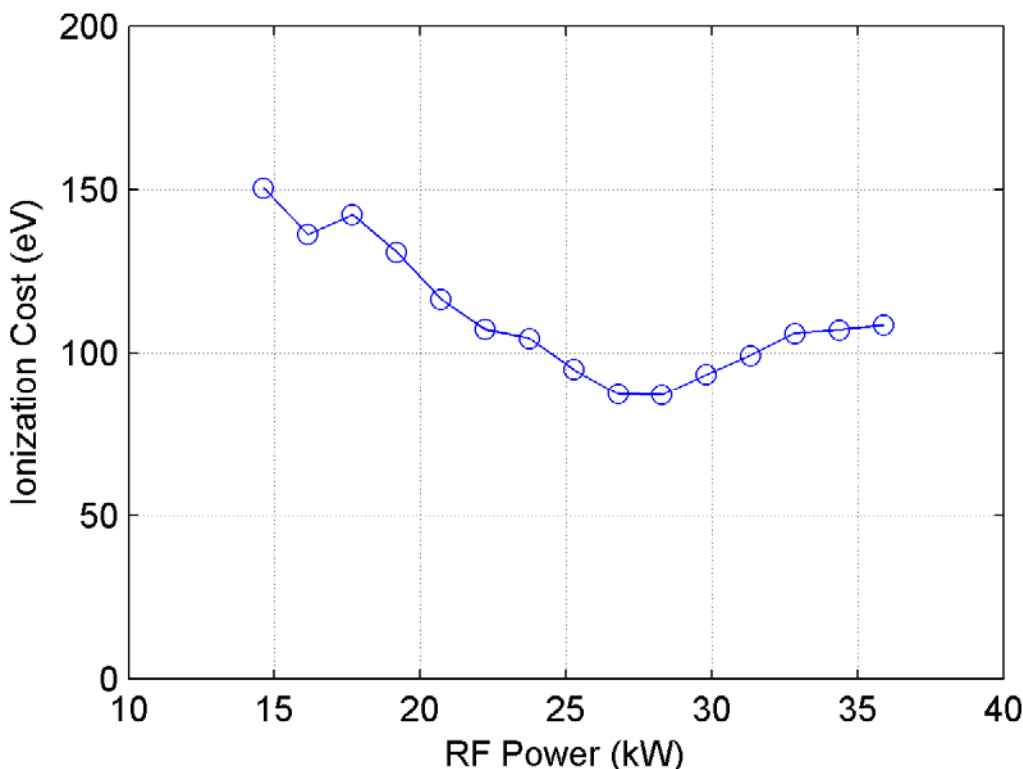
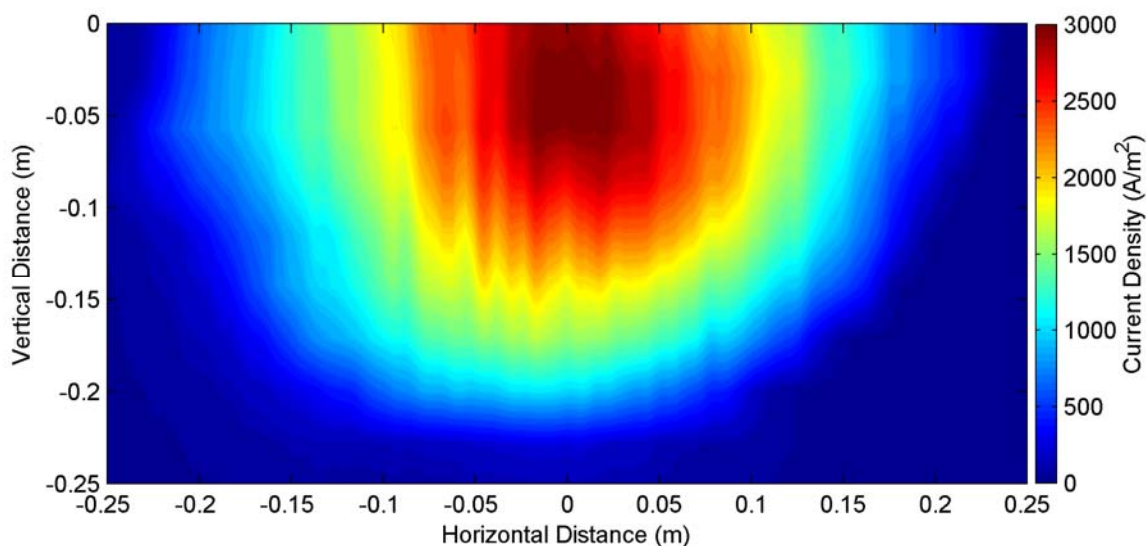
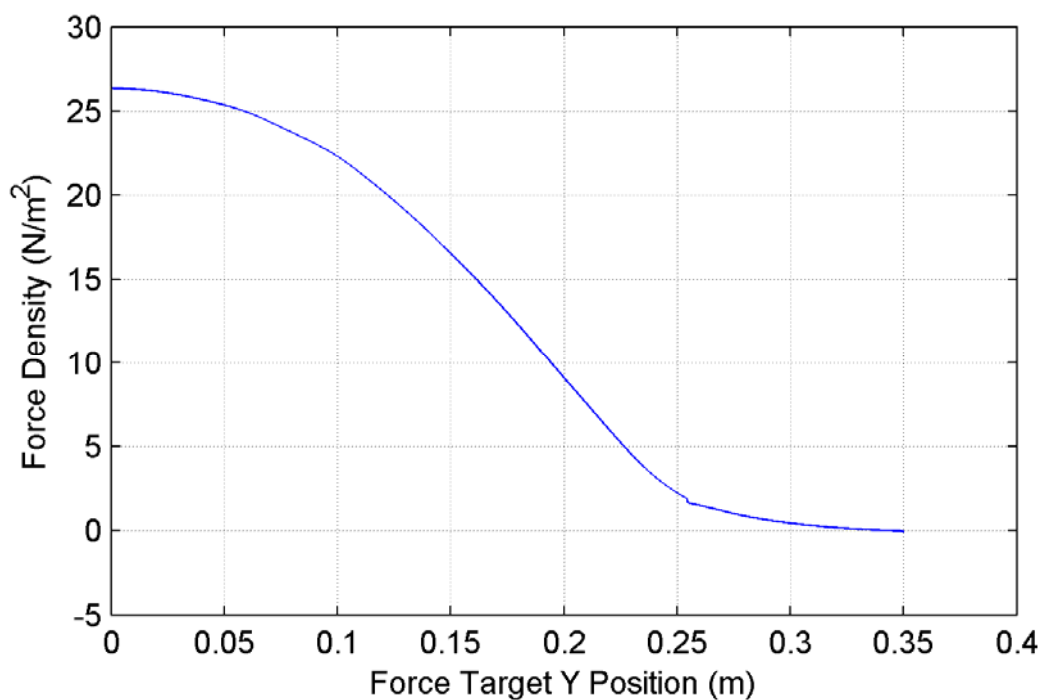


**Figure 11. The minimum ionization cost as a function of helicon RF coupled power. The uncertainty of the ionization cost is 10%.**

an indication of the ion energy distribution as a function of radial location in the exhaust plume. In fact, the ion energy distribution is relatively flat across the diameter of the exhaust plume.



(a) Current density map for helicon-only operation. The axes are relative to the axis of the rocket. The flux density peak is slightly off-center, probably due to the diagnostic translation stage blocking a fraction of the plume below the axis.



(b) A horizontal force density profile.

**Figure 12. Force profile and current density map of helicon operation. The ionization cost is determined from the RF power. The energy in the ions determined from the force.**

#### IV. Plasma Pulses

In order to accommodate advances in low-mass solid-state RF power generation in anticipation for spaceflight, new proprietary algorithms had to be developed for successful high-power startup. Some of the first recipes involved active tuning of the RF circuit over several seconds before acceptable helicon modes were achieved (Figure 13a). These methods recently have been drastically improved resulting in fast (<50 ms) coupling of the helicon mode into the plasma (Figure 13b). Improvements can still be made, however, neutral gas dynamics will ultimately limit the startup time when the distance between the fuel reservoir and ionization chamber must be taken into account.

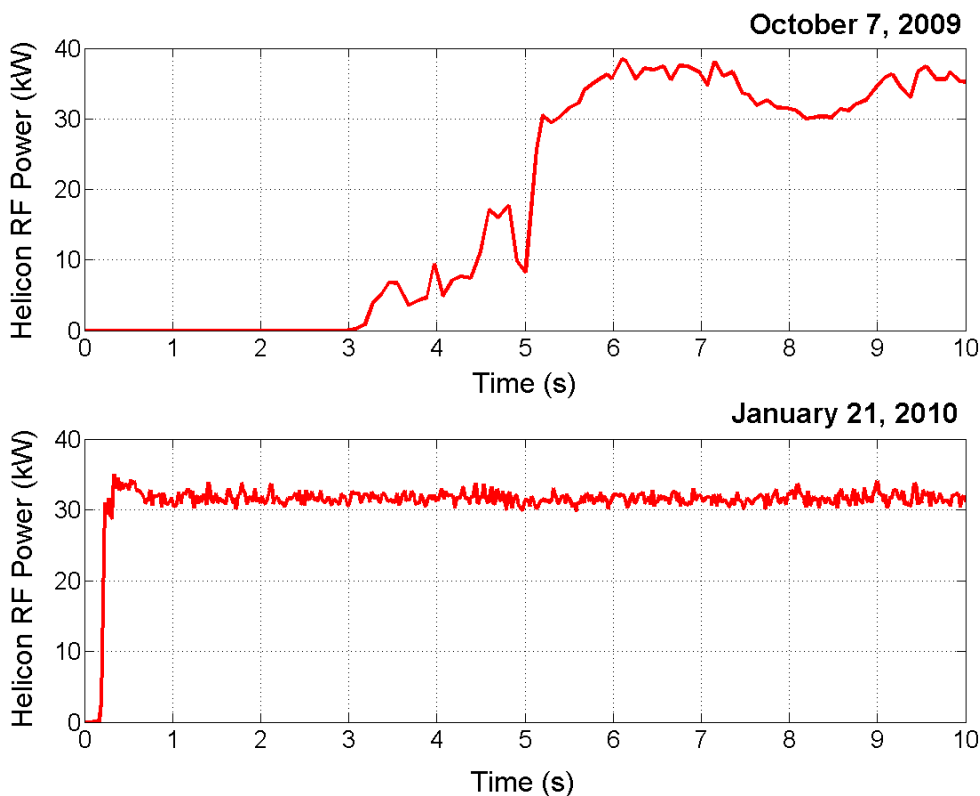


**Figure 13. Comparison of the time for the helicon to reach steady state operation. (a) Helicon RF power startup temporal profile with active tuning. (b) Helicon RF power startup temporal profile with advanced tuning.**

The neutral pressure has been measured in the chamber as shown in Figure 14. The pressure data indicate that the charge exchange mean free path was ~100-120 cm during the first 800 ms, and then 10 cm during steady-state operations.

#### V. Experimental Momentum Flux Results

##### A. VX-200 Momentum Flux Measurements

The VX-200 achieved full rated operating power of 200 kW dc power in to the ICH RF transmitters on Sept. 30, 2009. During the next month, an experiment campaign began mapping the exhaust plume to evaluate the output of the thruster. The team is still in the process of refining instrument cross calibration. Thruster overall performance is in a preliminary stage, and several major improvements are planned. Thus, all results reported here are in arbitrary units and must be regarded as preliminary.

Contour maps of the momentum flux density in the exhaust plume of the VX-200 are shown in Figures 15 and 16. These maps were constructed by interpolating the PMFS data taken on a regular 10 cm grid during separate plasma shots. The origin of the  $z$  (or axial) coordinate is the edge of the end cap vacuum flange. The end of the motor nozzle is at 2.6 m on this scale. Several major points stand out in these figures. The helicon only plume produces orders of magnitude more force than a neutral gas jet with the same mass flow rate. The ICH increases the force level by a factor of at least 5. The boundary of the plume is essentially a straight line. This pattern is taken as evidence that the exhaust plume is detaching from the magnetic field. Finally, the thrust density falls off exponentially with distance from the nozzle. The e-folding distance of this decay is

consistent with the charge exchange mean free path owing to resonant charge exchange with the neutral background that builds up in the chamber during each shot. Thus, this fall-off is a laboratory effect that will not occur in flight.

The sharply collimated nature of the thrust and plasma in the exhaust plume were further studied by constructing a comparison plot of the thrust density and ion flux data taken on one of the innermost radial scans ( $z = 2.9$  m). Cylindrical symmetry was assumed. The results have been plotted in a trimetric wire frame view shown in Figure 17. Two features stand out. The inner core of the ion flux is sharply peaked, with a shoulder at about  $r \sim 0.15$  m. The thrust density profile is broader in the center than the flux density, but then falls off more steeply at the edge. This columnar geometry is required for high nozzle efficiency and is consistent with plasma detachment. The cause of the shoulder in the flux profile is unknown and under investigation.

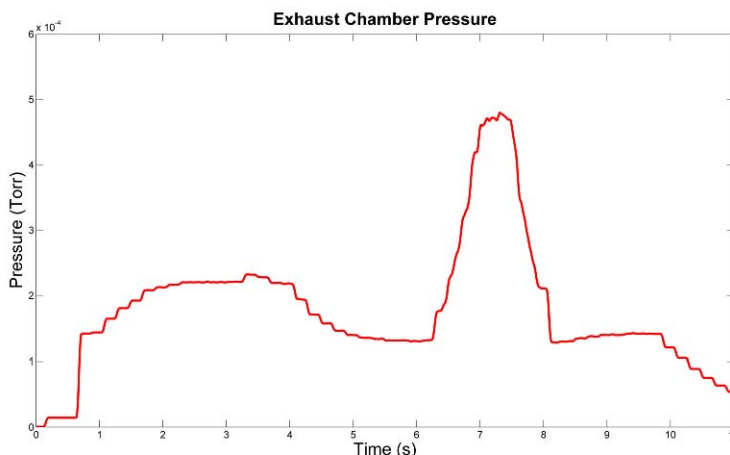


**Figure 14. Representative downstream chamber pressure during the VX-200 firings. Pressure was measured and digitized using a Granville-Phillips micro-ion plus gauge. The pressure in the exhaust chamber never goes above mid  $10^{-4}$  Torr throughout the duration of the shot. This pressure is well over an order of magnitude lower than the VX-100 device. At these pressures, the charge exchange mean free path is approximately 100 – 120 cm.**

## VI. General VX-200 Results

### A. Power Data

The VX-200 achieved design full power operation on Sept. 30, 2009. The total dc power delivered to the RF amplifiers is shown in Figure 18. The ICH amplifier was on from 4.6 to 5.2 s. The stepped turn-on ramp reflects the modular design of the amplifier and the modular sequencing of the turn-on process. The ability of the VX-200 to sustain high power operations for extended time intervals is demonstrated in Figure 19. The figure shows that the ICH amplifier operated at 120 kW for 5 s. Figure 19 demonstrates that the RF system is capable of sustained high power operation.

## Axial Force Contour Map (Steady Helicon)

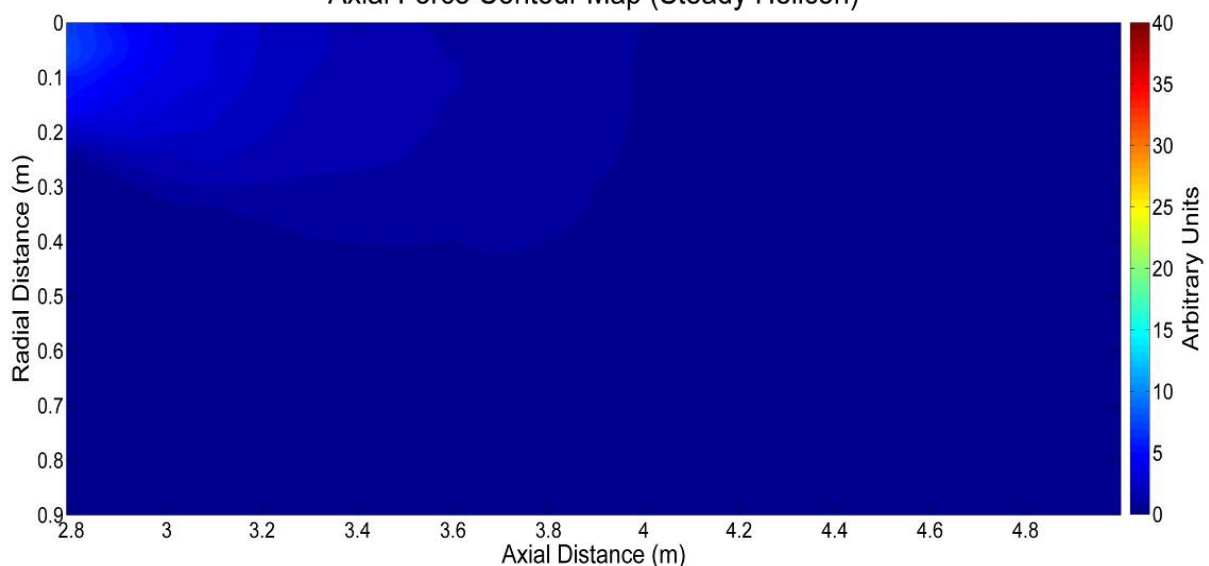


Figure 15. VX-200 helicon plume map based on data from the PMFS graphite target. Exact units are intentionally left off pending further calibration. Data were taken over several radial passes of the 2 axis translation stage. The first stage Helicon discharge produces noticeable force above a low flow neutral gas jet.

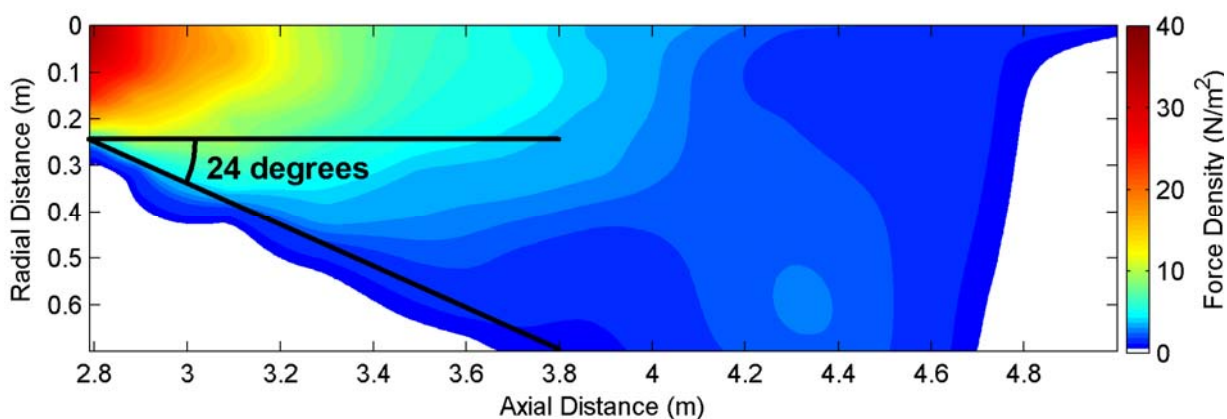


Figure 16. VX-200 full power plume map based on data from the PMFS graphite target. The data in this figure were taken approximately 3 s after the data in Figure 15. The peak force increases by a factor of 5 with the addition of approximately 145 kW of RF power. This demonstrates that the momentum flux in the plume of the VASIMR<sup>®</sup> is well defined and directed downstream of the rocket engine. The half-angle of 24 degrees within which 90% momentum is contained is shown.

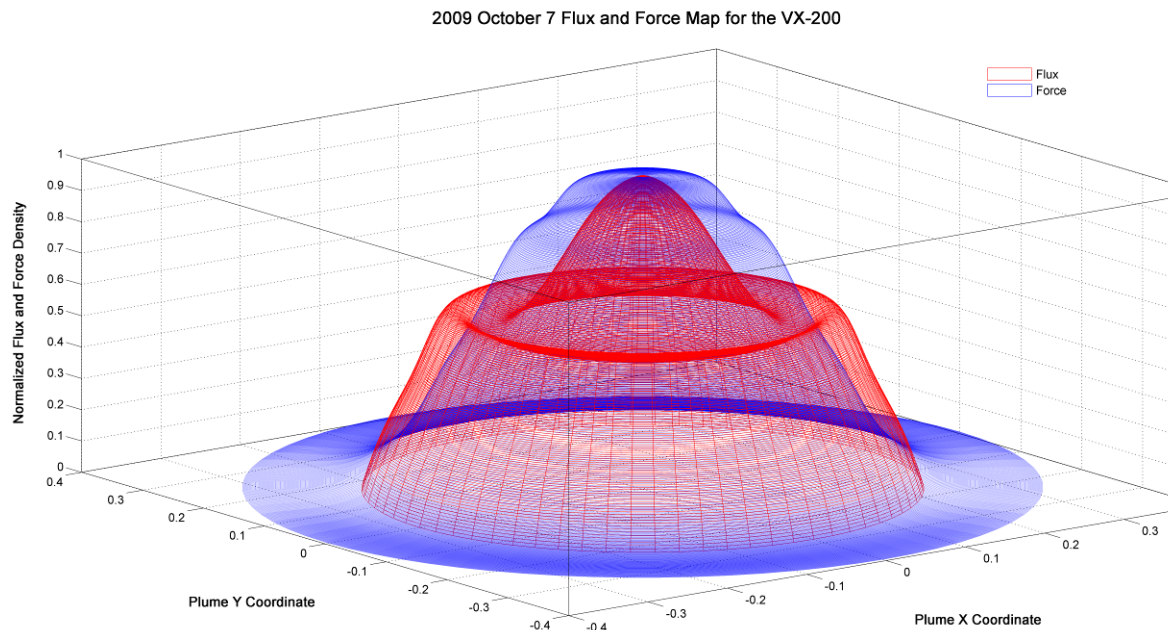


Figure 17. Force density (blue) and ion flux data from a  $z = 2.9$  m radial scan are plotted in a trimetric view of plume structure assuming cylindrical symmetry.

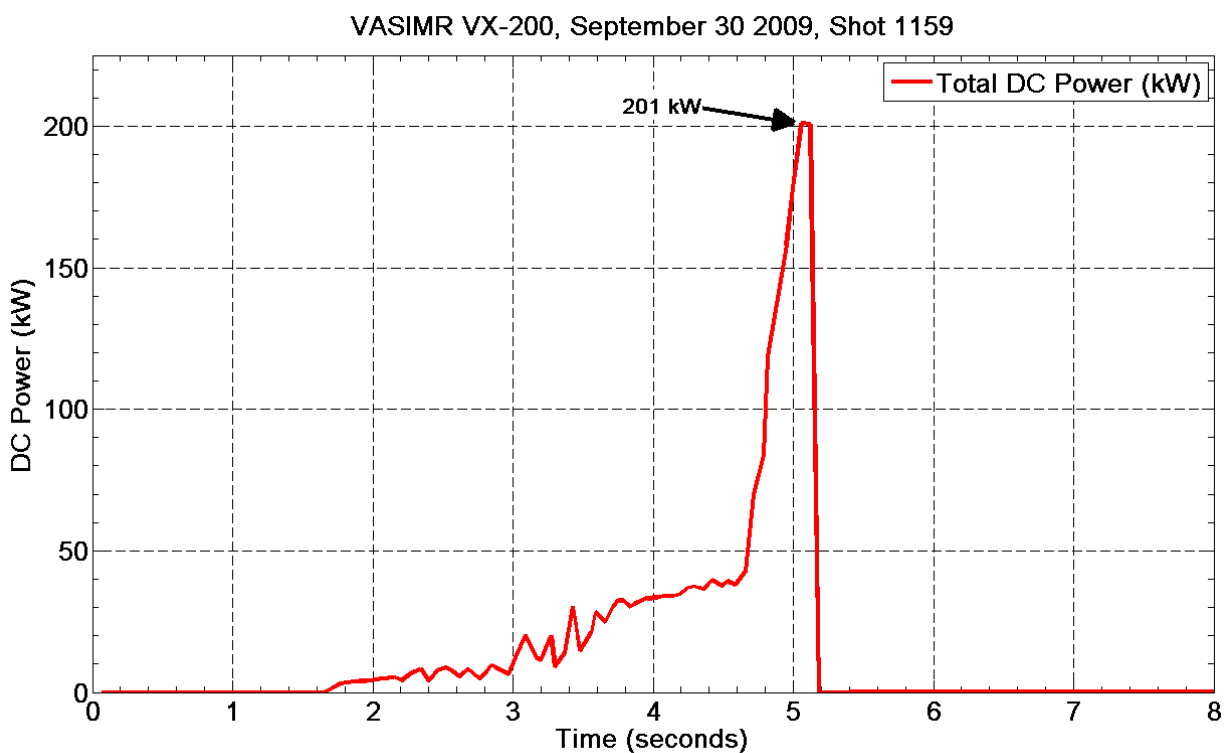


Figure 18. Total DC power to the VASIMR RF amplifiers plotted as a function of time during the first shot that achieved design full power. The helicon amplifier operated at 35 kW, and the ICH amplifier operated at 166 kW.

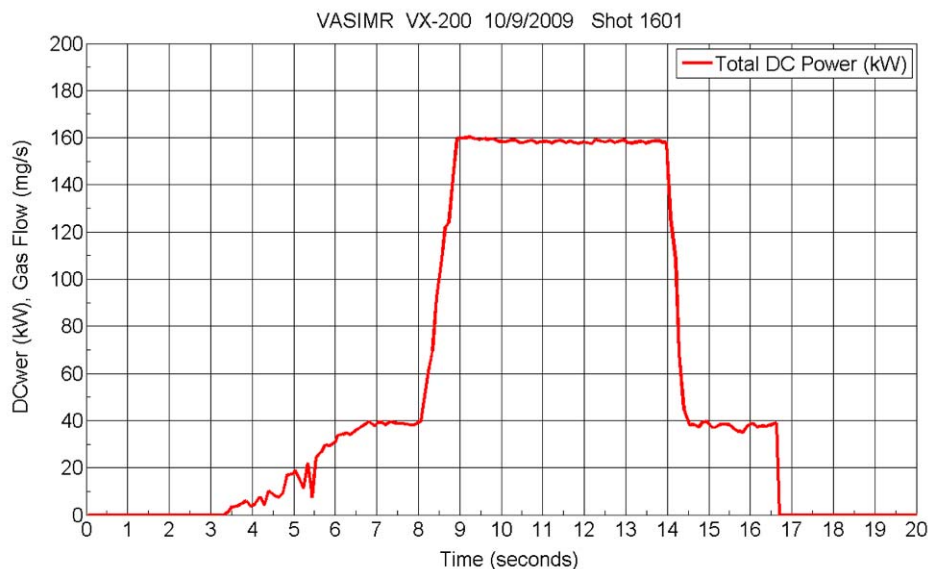


Figure 19. Total power curve for a shot where ICH operation was sustained for 5 s.

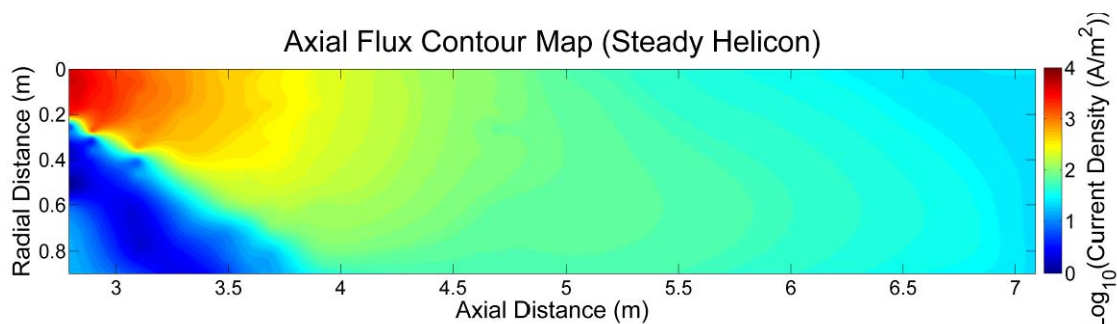


Figure 20. VX-200 ion flux map (first stage Helicon only) based on Langmuir Probe data. The small planer molybdenum probe was steadily biased into ion saturation (- 30 V). The plume is slightly asymmetric and the ions are affected by charge exchange.

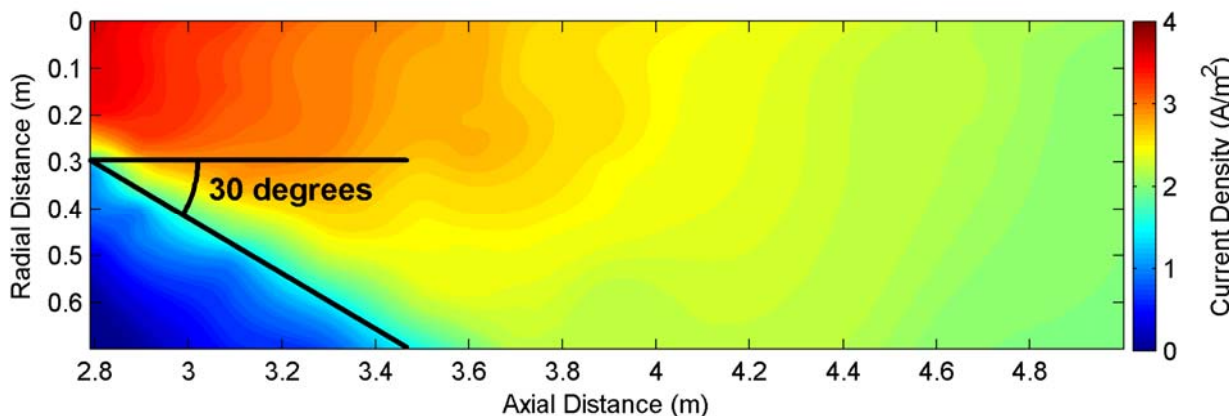
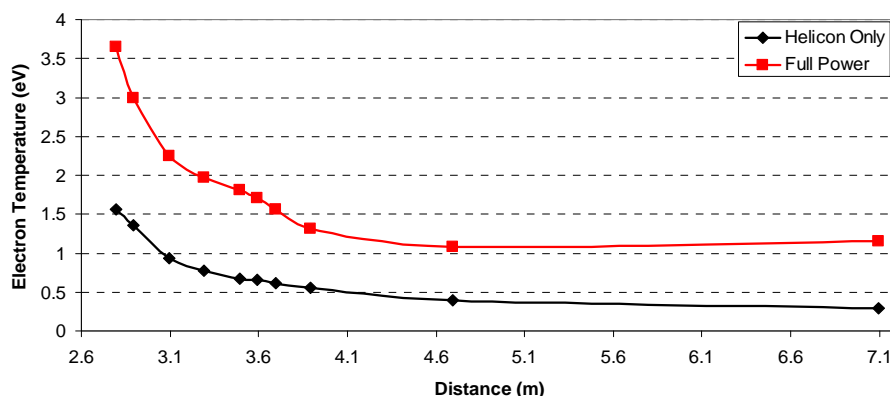


Figure 21. VX-200 ion flux map (Full power Helicon and ICRF) based on Langmuir probe data. The data in this figure are taken approximately 3 seconds after the data from Figure 17. The plume is slightly broader than with Helicon only as well as better defined along the edges. More ion flux propagates downstream despite a higher exhaust chamber pressure since the increased ion energy corresponds to a larger charge exchange mean free path.



**Figure 22. Axial scan comparison of the Helicon only (~ 35 kW) and full power (~ 170 kW) measured Electron Temperature. The data were extracted using a swept Langmuir Probe. The electron temperature increases approximately 1 to 3 eV with the addition of 140 kW RF power.**

## B. Plasma Data

Ion flux maps of the VX-200 plasma plume are shown in Figures 20 and 21. The contour maps are based on planar Langmuir probe data taken in one location per plasma shot. An extended campaign of a week's duration was required to make 10-cm step radial scans at several axial distances. Contour maps were constructed using standard 2-D

interpolation

techniques. Two points stand out. First, the plume has a sharp, relatively straight outer boundary, which we take to indicate that the plasma plume is detaching and not following magnetic field lines. Second, the ICH plume extends further downstream than the helicon only plume, which appears to show a greater charge exchange mean free path for the higher energy ions.

The VASIMR design objective is to maximize energy input into the ions and only to energize the electrons to the extent required to achieve full ionization. The design then retrieves some of this heat via ambipolar ion acceleration in the inner part of the exhaust plume. Nonetheless, when operating at power levels >120 kW in the ICH, it is hard to avoid putting *some* energy into the electron population. Figure 22 shows an axial scan of electron temperature, comparing helicon only with ICH full power. Data were taken in the same shots 3 s apart. Close to the VASIMR, the electron temperature was increased by 3 eV, which was nearly a factor of 3. This increase was reflected in an equivalent increase in plasma potential, as shown in Figure 23. The decrease in electron temperature with increasing axial distance reflects the loss of energy to the ion flow speed via ambipolar acceleration.

The ICH boost is intended to provide an efficient method of accelerating the ions. This acceleration is misnamed "heating." The process is deterministic and affects only one degree of freedom. The effect of the ICH on the ions in the VX-200 is explored in Figures 24-26. Figure 24 shows a trimetric wireframe view of the ion energy distributions from the RPA located on the centerline at  $z = 2.9$  m, plotted as a function of both ion energy and ICH power, all normalized. The ion energy increases from a peak at ~50 eV produced by the helicon plus ambipolar acceleration to ~180 eV at full ICH power. This level is lower than intended for the VF-200, owing to deliberate, temporary use of a sub-optimal ICH coupler for initial tests. There was also a residual low energy peak, indicating that either that charge exchange was acting to produce a low energy, cool ion population or that the only part of the ion population was accelerated.

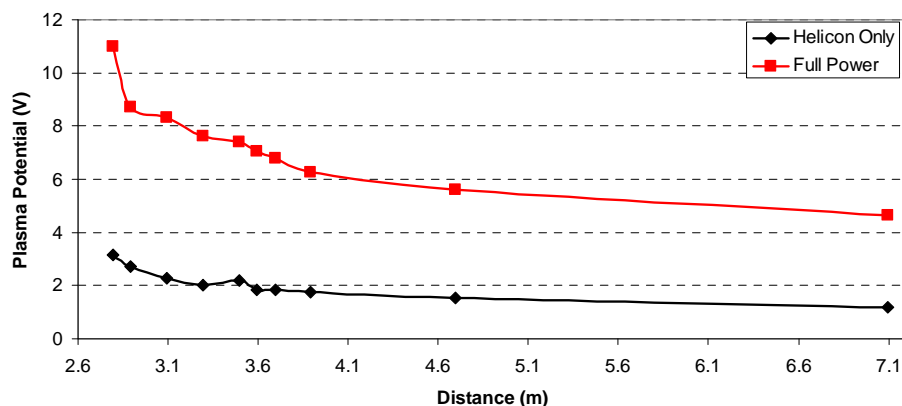


**Figure 23. Axial scan comparison of Helicon only (~ 35 kW) and full power (~ 170 kW) measured plasma potential. The data were extracted using a swept planer Langmuir probe. The increase in power raises  $V_p$  4- 8 volts.**

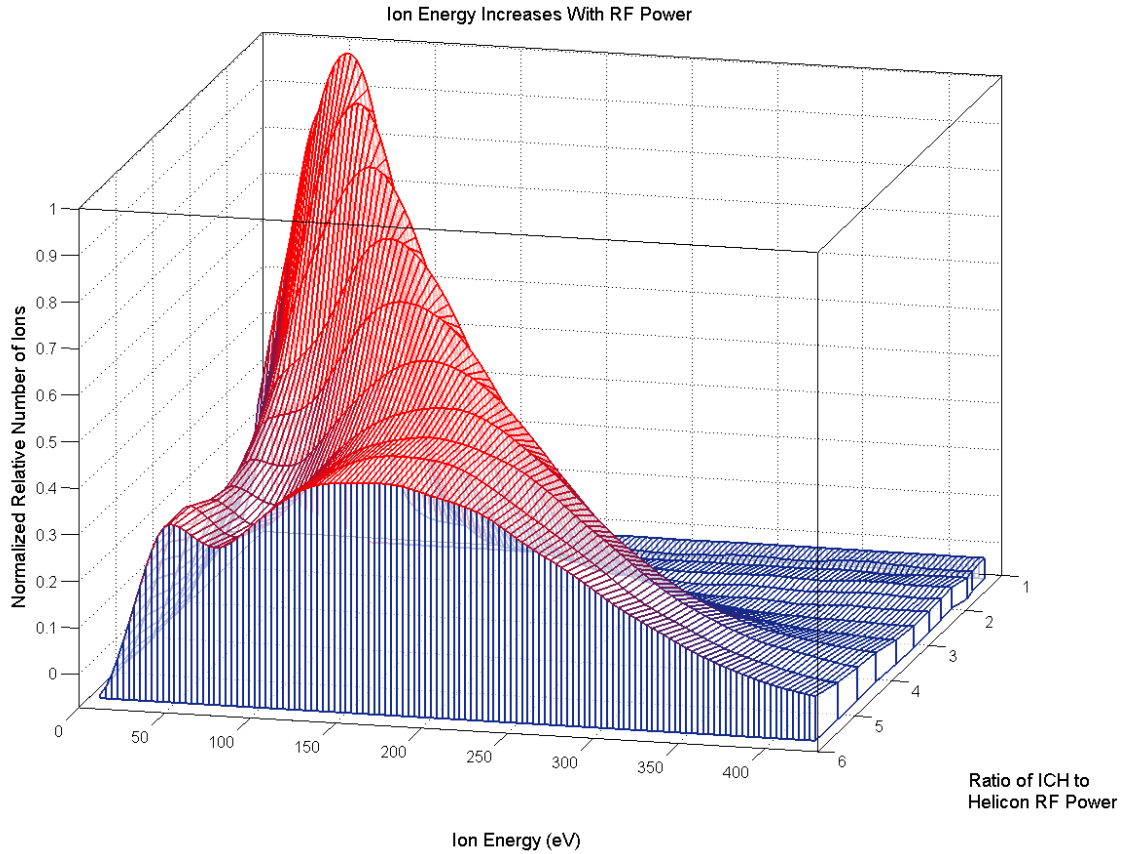


**Figure 24. Ion energy distribution function measured by the RPA at an axial distance  $z = 2.9$  m, showing a trimetric wire-frame view of the evolution of the ion energy distribution as ICH power increases.**

Figure 25 shows a comparison of contour plots of the 2-D ion velocity phase space distribution function for ICH on vs ICH off. These data were obtained at  $z = 4.4$  m, which is 2 m downstream from the ICH resonance. The measurements were made using the powered angle scan mount of the RPA, moving the translation stage so as to keep the RPA in one place. These figures show two things. First, the accelerated ion jet is tightly collimated in velocity space. Second, at this distance, the unaccelerated component shows evidence of a substantial amount of elastic scattering to higher pitch angles.

Figure 26 shows the fit parameters inferred by least squares fitting drifting Maxwellians to the RPA I-V characteristics: parallel ion temperature in the frame of the beam, drift velocity, and an uncalibrated parameter corresponding to density. Panel (a) shows an axial scan, with the RPA at a radius of -0.178 m. Panel (b) shows a diameter scan at  $z = 3.6$  m. The VASIMR nozzle exit is located at  $z = 2.6$  m. Two striking things jump out of this figure. The density decays exponentially, with an e-folding distance of 1.2 m, which is consistent with charge exchange as the loss mechanism. The apparent ion acceleration near the nozzle may be ambipolar acceleration. However, it is probably the result of the location of the RPA off the centerline. At the closest distances, it was in the fringe of the plume.

## VII. Thruster Efficiency

The VX-200 thruster efficiency is determined by dividing the total RF power coupled to plasma by the thruster jet power. The jet power is defined as

$$P_{jet} = \frac{F^2}{2\dot{m}}, \quad (3)$$

where  $F$  is the total force produced by the rocket and  $\dot{m}$  is the total mass flow rate of propellant. The force from VX-200 was determined by using a force impact target that measured the local force density within the exhaust plume as a function of radial position. The force density over one full diameter of the exhaust plume was integrated, with the assumption of azimuthal symmetry, in order to determine the total force produced by the VX-200. The force density diameter profile was taken 40 cm downstream from the end of the VX-200 thruster. This force measurement location is approximately 30 cm downstream of the magnetic nozzle, where the end of the magnetic nozzle is defined as the point where 90% of the perpendicular ion momentum has been converted to parallel momentum along the axis of the thruster, a process described by conservation of the first adiabatic invariant. The force target is 9 cm in diameter, small compared to the total exhaust plume diameter of approximately 50 cm, and has a resolution of 0.1 mN. Dividing equation 3 by the total RF power coupled to the plasma gives

$$\eta_T = \frac{P_{jet}}{P_{1,RF} + P_{2,RF}}, \quad (4)$$

where  $P_{1,RF}$  and  $P_{2,RF}$  represent the RF power coupled to the first and second stage plasma, respectively.

An experiment campaign in May of 2010 that used a propellant flow rate of 107 mg/s yielded results that show a total force of up to 3.6 N and 54% efficiency at a total coupled RF power of 108 kW. The specific impulse was calculated using the total force measurement and a propellant mass flow rate measurement where

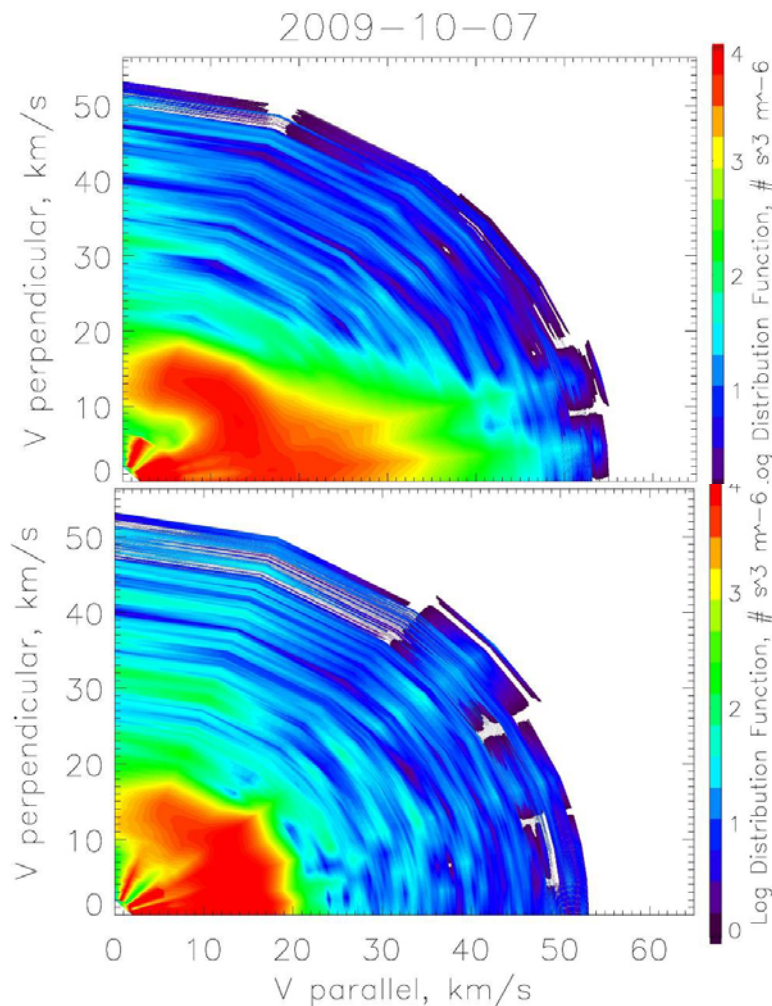
$$I_{sp} = \frac{F}{\dot{m}g}, \quad (5)$$

Figure 27 displays the thruster efficiency of the VX-200 as a function of the specific impulse of VX-200. The Helicon stage is left at a constant 28 kW, while the ICH stage power is varied from 0 to 81 kW. The limiting factor in the maximum applied RF power to the VX-200 in this experiment campaign was a vacuum pressure limit within the vacuum chamber, where greater RF circuit voltages produced glow or arc discharges which prompted the solid state RF generators to shut down. Standard high voltage conditioning techniques are used to mitigate these risks and a push for higher power levels at lower pressure is forthcoming in future experiment campaigns. The efficiency continues to increase as a function of applied ICH RF power, indicating that the process of ICH wave coupling into the plasma column has not saturated.

The relation between efficiency and specific impulse is an important design metric that we have been working to measure. We are extremely satisfied with greater than 50% efficiency at as low as 3000 s  $I_{sp}$  for this experimental device. A semi-empirical model is also graphed in Figure 27, and is a least squares fit to the data using ICH coupling efficiency as a free parameter. The free and fixed (measured) parameters of the model were explained in a previous publication<sup>38</sup>. Retarding potential energy analyzer data taken during the campaign corroborates the determined ion energy to within 10% at high ICH power levels. Figure 27 also indicates that the ICH wave coupling process is not saturated, as the efficiency of the VX-200 continues to increase with increasing applied ICH power. The VX-200 helicon and ICH couplers were designed to produce a thrust efficiency of 60% at 5000 s, and the data indicate that the VX-200 is more efficient than the original design goal.

## VIII. Conclusions

For the first time, a thrust efficiency and force of a high-power VASIMR<sup>®</sup> with good vacuum conditions has been presented. The efficiency was measured to be between 50% and 54% with the specific impulse in the range of 3000 to 3500 s. A maximum force of 4.4 N was measured at 40% thrust efficiency. The ionization cost was determined to be 87 eV for optimized values of RF power and propellant flow rate. A semi-empirical model predicts a thrust efficiency of 64% at 6000 s and 200 kW. The VX-200 has produced a massive amount of new data that is helping narrow the design for a flight unit. Ad Astra Rocket Company is continuing to study and improve the operation of the VASIMR<sup>®</sup> engine through testing of the VX-200. We will modify the coupler designs until we can reliably reach 200 kW total power. Recently the vacuum chamber was upgraded for continuous pumping by three cryopanels and a fourth should come on line later this year. The improved vacuum conditions will allow for more accurate measurements of plume properties a few meters downstream. One of the primary experimental goals over the next year will be to demonstrate plasma detachment with detailed measurements of the plasma plume.



**Figure 25. Ion velocity phase space distribution function measured at  $z = 4.4$  m and  $y = 0$ . (a) Top panel shows ICH on. (b) Bottom panel data were taken 3 s earlier, before ICH turned on.**

The VX-200 is now operating with superconducting magnets and has achieved full design power. The plasma exhaust plume of the VX-200 has properties and structure that demonstrate that the VX-200 is approaching full design performance. A further factor of 2 increase in ion acceleration efficiency is possible. The geometry of the plume is consistent with the occurrence of plasma detachment. The plasma is moving ballistically and does not appear to be following the magnetic field lines. Neutral gas build-up is observed to reduce charge exchange mean free path to  $\sim 1$  m. The neutral gas imposes limits on the verisimilitude of the experimental simulation of in space operation. A better demonstration of detachment will require first operation of all four cryopump panels and later space testing.

### Acknowledgments

The authors (B.L.) would like to thank the University of Houston Institute for Space Systems Operations (ISSO) postdoctoral fellowship program for partial support of this research. NASA Johnson Space Center under grant NAG 9-1524, the Texas Higher Education Coordinating Board under Advanced Technology

Program project 003652-0464-1999 and the Ad Astra Rocket Company sponsored this research.

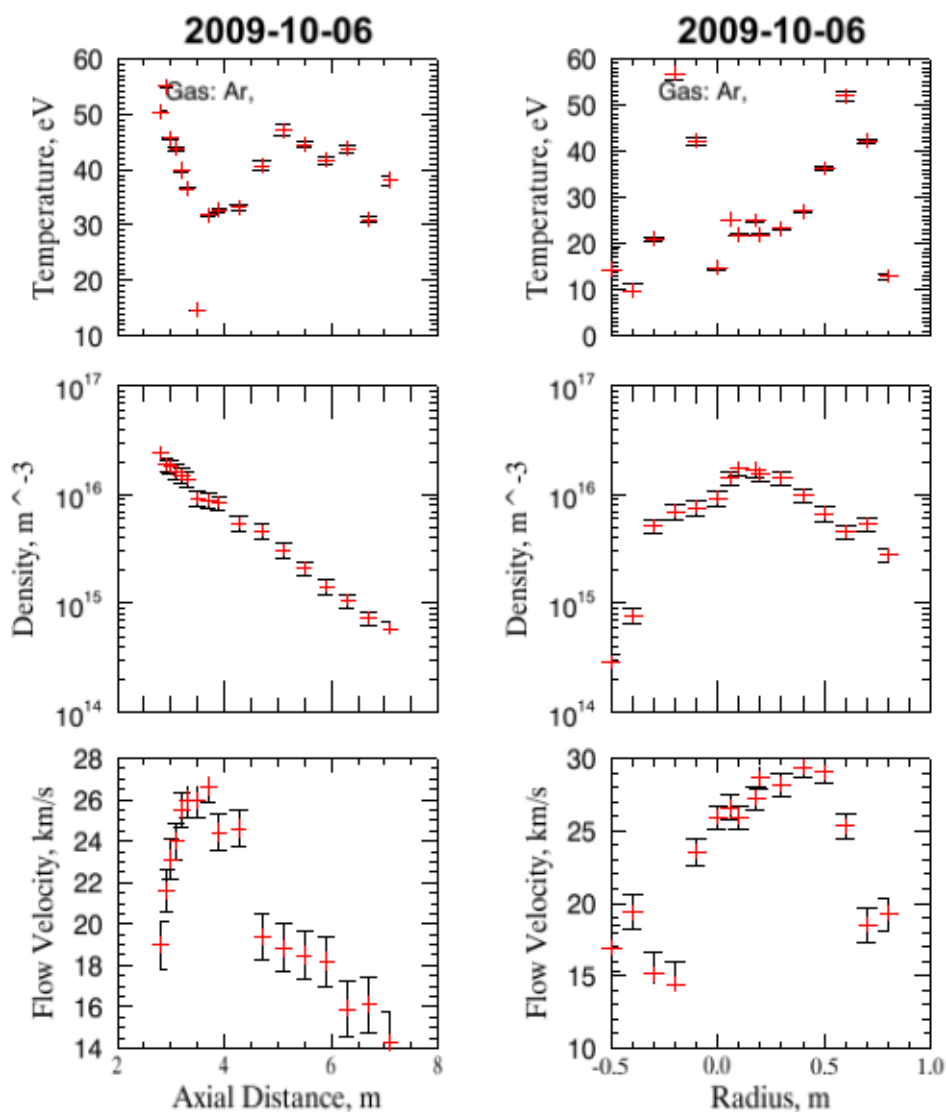


Figure 26. Parameters inferred from least squares fitting a drifting Maxwellian to RPA data. From top to bottom, panels show parallel ion temperature in the frame of the beam, ion density (uncalibrated, arbitrary units) and ion flow velocity. (a) Axial plot. Origin of the  $z$ -axis is at the edge of the upstream end of the vacuum chamber. Motor nozzle is at  $z = 2.6$  m. All data were taken with the RPA at  $y = -0.178$  m when stage  $y = 0$ . (b) Radial plot. RPA is on center at  $y = 0.178$  m. This diameter scan was at  $z = 3.6$  m.

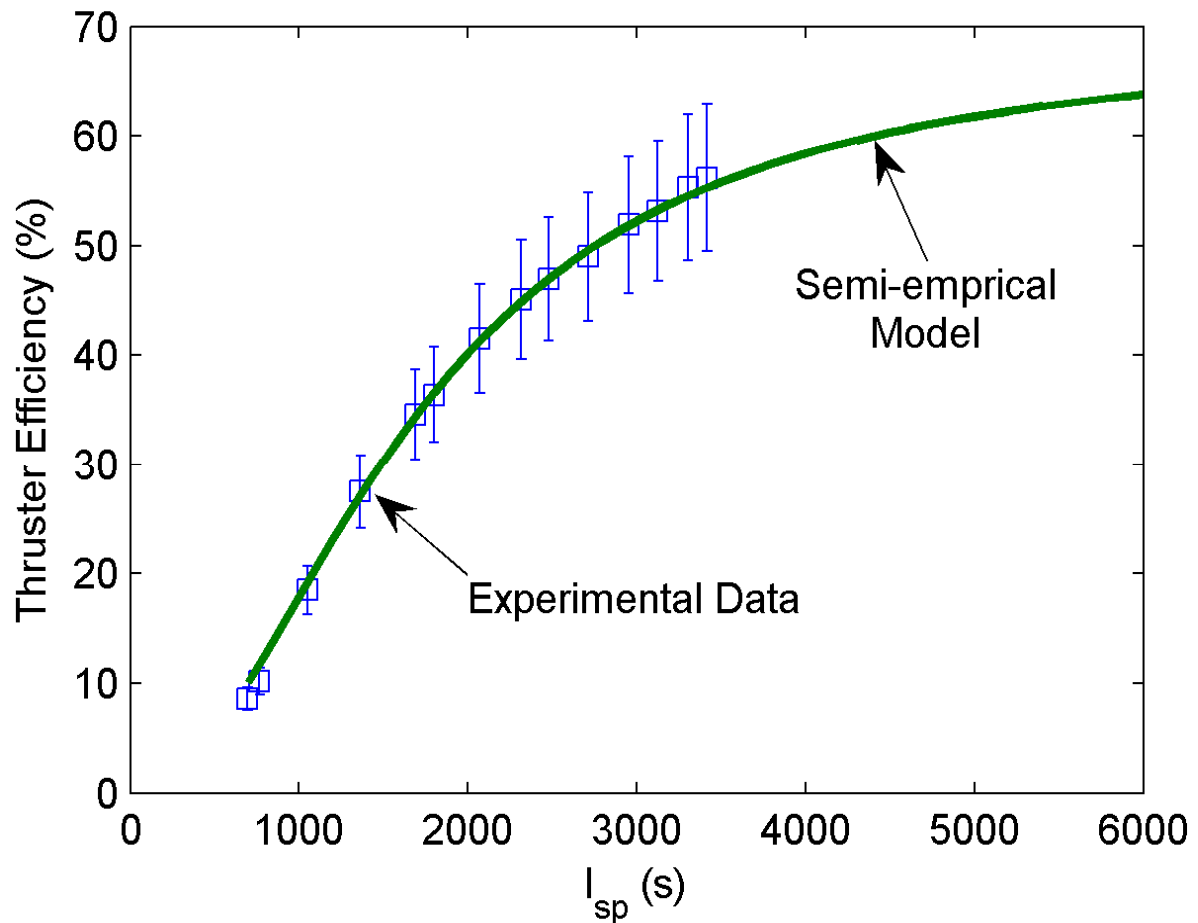


Figure 27. Measured efficiency as a function of specific impulse compared to a semi-empirical model.

## References

- <sup>1</sup> Sankaran, K., Cassady, L., Kodys, A., and Choueiri, E., "A Survey of Propulsion Options for Cargo and Piloted Missions to Mars," *Astrodynamics Space Missions and Chaos*, edited by E. Belbruno, D. Folta, and P. Gurfil, Vol. 1017, Annals of the New York Academy of Sciences, New York, NY, USA, 2004, pp. 450-567.
- <sup>2</sup> Frisbee, R., "SP-100 Nuclear Electric Propulsion for Mars Cargo Missions," *29th AIAA/SAE/ASME/ASEE Joint Propulsion Conference*, Monterey, CA, USA, June 1993, AIAA-93-2092.
- <sup>3</sup> Frisbee, R., "Electric Propulsion Options for Mars Cargo Missions," *32nd AIAA/ASME/SAE/ASEE Joint Propulsion Conference and Exhibit*, Lake Buena Vista, FL, USA, July 1996, AIAA-96-3173.
- <sup>4</sup> Polk, J. and Pivirotto, T., "Alkali Metal Propellants for MPD Thrusters," *AIAA/NASA/OAI Conference on Advanced SEI Technologies*, Cleveland, OH, USA, September 1991, AIAA-91-3572.
- <sup>5</sup> Glover, T., Chang Díaz, F. R., Ilin, A. V., and Vondrak, R., "Projected Lunar Cargo Capabilities of High-Power VASIMR<sup>®</sup> Propulsion," *30th International Electric Propulsion Conference*, September 2007, IEPC-2007-244.
- <sup>6</sup> Ilin, A., Cassady, L., Glover, T., Carter, M., and Chang Díaz, F., "A Survey of Missions using VASIMR<sup>®</sup> for Flexible Space Exploration," Tech. Rep. JSC-65825, NASA - JSC, April 2010.
- <sup>7</sup> Boswell, R. W. and Chen, F. F., "Helicon: The early years," *IEEE Transactions of Plasma Science*, Vol. 25, December 1997, pp. 1229-1244.
- <sup>8</sup> Chen, F. F. and Boswell, R. W., "Helicon: The past decade," *IEEE Transactions of Plasma Science*, Vol. 25, December 1997, pp. 1245-1257.
- <sup>9</sup> F. R. Chang Díaz, J. P. Squire, T. Glover et al., "VASIMR<sup>®</sup> Engine: Project Status and Recent Accomplishments, The," presented at the *42nd AIAA Aerospace Sciences Meeting and Exhibit*, Reno, NV, 2004.

- <sup>10</sup> F. R. Chang Díaz, "An overview of the VASIMR<sup>®</sup> engine: High power space propulsion with RF plasma generation and heating." Presented at the *14th Topical Conference on Radio Frequency Power in Plasmas*, May 7-9, Oxnard, CA, 2001 (unpublished).
- <sup>11</sup> R. W. Boswell, "Very efficient plasma generation by whistler waves near the lower hybrid frequency." *Plasma Phys. Control. Fusion*, 26, 1147 (1984).
- <sup>12</sup> F. F. Chen, "Plasma ionization by helicon waves." *Plasma Physics and Controlled Fusion*, 33(4), 339-364 (1991).
- <sup>13</sup> R. W. Boswell and C. Charles, "The helicon double layer thruster." Presented at the *28th International Electric Propulsion Conference, IEPC 2003*, Toulouse, France, 2003.
- <sup>14</sup> S. N. Golovato, K. Brau, J. Casey et al., "Plasma Production and Heating in a tandem mirror central cell by radio frequency waves in the ion cyclotron frequency range," *Phys. Fluids*, 3 (12), 3744-3753 (1988).
- <sup>15</sup> Y. Yasaka, R. Majeski, J. Browning et al., "ICRF heating with mode control provided by a rotating field coupler," *Nuclear Fusion*, 28, 1765 (1988).
- <sup>16</sup> Squire, J. P., Chang Díaz, F. R., Carter, M. D., Cassady, L. D., Chancery, W. J., Glover, T. W., Jacobson, V. J., McCaskill, G. E., Bengtson, R. D., Bering, E. A., and Deline, C. D., "High Power VASIMR<sup>®</sup> Experiments using Deuterium, Neon and Argon," *30th International Electric Propulsion Conference*, September 2007, IEPC-2007-181.
- <sup>17</sup> Squire, J., Chang Díaz, F., Glover, T., Carter, M., Cassady, L., Chancery, W., Jacobson, V., McCaskill, G., Olsen, C., Bering, E., Brukardt, M., and Longmier, B., "VASIMR<sup>®</sup> Performance Measurements at Powers Exceeding 50 kW and Lunar Robotic Mission Applications," *International Interdisciplinary Symposium on Gaseous and Liquid Plasmas*, Akiu/Sendai, Japan, September 2008.
- <sup>18</sup> Bering, E., Chang Díaz, F., Squire, J., Glover, T., Carter, M., McCaskill, G., Longmier, B., Brukardt, M., Chancery, W., and Jacobson, V., "Observations of single-pass ion cyclotron heating in a trans-sonic flowing plasma," *Physics of Plasmas*, Vol. 17, No. 4, 2010.
- <sup>19</sup> Cassady, L., Chancery, W., Longmier, B., Squire, J., Carter, M., Glover, T., Olsen, C., Ilin, A., McCaskill, G., Chang Díaz, F. R., and Bering, E., "VASIMR Technological Advances and First Stage Performance Results," *45<sup>th</sup> AIAA/ASME/SAE/ASEE Joint Propulsion Conference and Exhibit*, August 2-5 2009, AIAA 2009-5362.
- <sup>20</sup> Squire, J., Cassady, L., Chang Díaz, F., Carter, M., Glover, T., Ilin, A., Longmier, B., McCaskill, G., Olsen, C., and Bering, E., "Superconducting 200 kW VASIMR<sup>®</sup> Experiment and Integrated Testing," *Proceedings of the 31st International Electric Propulsion Conference*, Ann Arbor, MI, September 20-24 2009, IEPC-2009-209.
- <sup>21</sup> Bering, E., Longmier, B., Chancery, W., Olsen, C., Squire, J., and Chang Díaz, F., "Exhaust plume spatial structure of the VASIMR<sup>®</sup> VX-200," *Proceedings of the 48th AIAA Aerospace Sciences Meeting*, Orlando, FL, January 4-7 2010, AIAA-2009-0622.
- <sup>22</sup> Bering, E., Longmier, B., Chang Díaz, F., Squire, J., Glover, T., Chancery, J., Carter, M., Cassady, L., and Brukardt, M., "VASIMR<sup>®</sup> VX-200: High power electric propulsion for space transportation beyond LEO," *Proceedings of AIAA Space 2009 Conference and Exposition*, Pasadena, CA, September 14-17 2009, AIAA-2009-6481.
- <sup>23</sup> V. I. Krassovsky, "Exploration of the upper atmosphere with the help of the third Soviet sputnik." *Proc. IRE*, 47, 289 (1959).
- <sup>24</sup> E. C. Whipple, "The ion trap-results in "Exploration of the upper atmosphere with the help of the third Soviet sputnik"." *Proc. IRE*, 47, 2023 (1959).
- <sup>25</sup> W. B. Hanson and D. D. McKibbin, "An ion-trap measurement of the ion-concentration profile above the  $F_2$  peak." *Journal of Geophysical Research*, 66, 1667 (1961).
- <sup>26</sup> L. W. Parker and E. C. Whipple, "Theory of spacecraft sheath structure, potential, and velocity effects on ion measurements by traps and mass spectrometers." *Journal of Geophysical Research*, 75, 4720-4733 (1970).
- <sup>27</sup> W. B. Hanson, S. Sanatani, D. Zuccaro et al., "Plasma measurements with the retarding potential analyzer on OGO 6." *Journal of Geophysical Research*, 75(28), 5483-5501 (1970).
- <sup>28</sup> W. B. Hanson, R. A. Heelis, R. A. Power et al., "The retarding potential analyzer for Dynamics Explorer-B." *Space Science Instruments*, 5, 503-510 (1981).
- <sup>29</sup> S. Minami and Y. Takeya, "Ion temperature determination in the ionosphere by retarding potential analyzer aboard sounding rocket." *Journal of Geophysical Research*, 87, 713 (1982).
- <sup>30</sup> B. W. Longmier, A. D. Gallimore, F. R. Chang-Díaz, J. P. Squire, T. W. Glover, D. G. Chavers, E. A. Bering III, and B. M. Reid, "Validating a plasma momentum flux sensor with a Hall thruster mounted on an inverted pendulum thrust stand," *J. Prop. Power*, doi: 10.2514/1.35706, 2009.
- <sup>31</sup> J. P. Squire, F. R. Chang-Díaz, R. Bengtson et al., "A plasma diagnostic set for the study of a variable specific impulse magnetoplasma rocket." Presented at the *APS Division of Plasma Physics Meeting*, Pittsburgh, PA, 1997 (unpublished).
- <sup>32</sup> Olsen, C., *Ion Flux Maps and Helicon Source Efficiency in the VASIMR VX-100 Experiment Using a Moving Langmuir Probe Array*, Master's thesis, Rice University, February 2009.
- <sup>33</sup> I. H. Hutchinson, *Principles of Plasma Diagnostics* (Cambridge University Press, Cambridge, 1987).
- <sup>34</sup> R. L. Stenzel, R. Williams, R. Aguero, K. Kitazaki, A. Ling, T. McDonald, and J. Spitzer, "Novel directional ion energy analyzer." *Review of Scientific Instruments*, 53 (7), 1027-1031 (1982).
- <sup>35</sup> R. L. Stenzel, W. Gekelman, N. Wild, J.M. Urrutia, and D. Whelan, "Directional velocity analyzer for measuring electron distribution functions in plasma." *Review of Scientific Instruments*, 54, 1302-1310 (1983).

---

<sup>36</sup> Chavers, D. and Chang-Díaz, F., “Momentum Flux Measuring Instrument for Neutral and Charged Particle Flows,” *Review of Scientific Instruments*, Vol. 73, No. 10, 2002.

<sup>37</sup> Longmier, B., Squire, J., Carter, M., Cassady, L., Glover, T., Chancery, W., Olsen, C., Ilin, A., McCaskill, G., Chang Díaz, F. R., and Bering, E., “Ambipolar Ion Acceleration in the Expanding Magnetic Nozzle of the VASIMR<sup>®</sup> VX-200i,” *45<sup>th</sup> AIAA/ASME/SAE/ASEE Joint Propulsion Conference and Exhibit*, August 2-5 2009, AIAA 2009-5359.

<sup>38</sup> Cassady, L., Longmier, B., Olsen, C., Ballenger, M., McCaskill, G., Ilin, A., Carter, M., Glover, T., Olsen, C., Ilin, A., Squire, J., Chang Díaz, F. R., and Bering, E., “VASIMR<sup>®</sup> Performance Results,” *46<sup>th</sup> AIAA/ASME/SAE/ASEE Joint Propulsion Conference and Exhibit*, July 25-28, 2010, AIAA 2010-6722.